



Title	Redox Behavior of In-O-Ti Interface for Selective Hydrogenation of CO <sub>2</sub> to CO in Doped In-TiO <sub>2</sub> Catalyst
Author(s)	Dostagir, Nazmul H. Md.; Fukuoka, Atsushi; Shrotri, Abhijit
Citation	ChemCatChem, 15(3), e202201348 <a href="https://doi.org/10.1002/cctc.202201348">https://doi.org/10.1002/cctc.202201348</a>
Issue Date	2023-02-08
Doc URL	<a href="https://hdl.handle.net/2115/91223">https://hdl.handle.net/2115/91223</a>
Rights	This is the peer reviewed version of the following article: [Dostagir, N. H. M., Fukuoka, A., Shrotri, A., ChemCatChem 2023, 15, e202201348.], which has been published in final form at <a href="https://doi.org/10.1002/cctc.202201348">https://doi.org/10.1002/cctc.202201348</a> . This article may be used for non-commercial purposes in accordance with Wiley Terms and Conditions for Use of Self-Archived Versions. This article may not be enhanced, enriched or otherwise transformed into a derivative work, without express permission from Wiley or by statutory rights under applicable legislation. Copyright notices must not be removed, obscured or modified. The article must be linked to Wiley's version of record on Wiley Online Library and any embedding, framing or otherwise making available the article or pages thereof by third parties from platforms, services and websites other than Wiley Online Library must be prohibited.
Type	journal article
File Information	In-TiO <sub>2</sub> _ChemCatChem 20221205.pdf



# Redox behavior of In–O–Ti interface for selective hydrogenation of CO<sub>2</sub> to CO in doped In–TiO<sub>2</sub> catalyst

Nazmul H. MD. Dostagir,<sup>[a]</sup> Atsushi Fukuoka,<sup>\*</sup> Abhijit Shrotri<sup>\*[a]</sup>

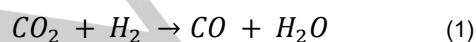
[a] Dr. N. H. MD. Dostagir, Prof. A. Fukuoka, Dr. A. Shrotri  
Institute for Catalysis  
Hokkaido University  
Kita 21 Nishi 10, Kita-ku, Sapporo, Hokkaido 001-0021, Japan  
E-mail: [ashrotri@cat.hokudai.ac.jp](mailto:ashrotri@cat.hokudai.ac.jp), [fukuoka@cat.hokudai.ac.jp](mailto:fukuoka@cat.hokudai.ac.jp)

Supporting information for this article is given via a link at the end of the document.

**Abstract:** In CO<sub>2</sub> hydrogenation reaction, selective synthesis of CO at low temperature and high pressure is needed to integrate the reverse water gas shift reaction with Fischer-Tropsch synthesis. Here, we show that a mixed oxide catalyst prepared by doping indium (In) into TiO<sub>2</sub> produces CO with the formation rate of 22 μmol g<sup>-1</sup> s<sup>-1</sup>. The CO selectivity was more than 99% at 350 °C and 3 MPa pressure. Moreover, the catalyst was durable for over 100 h on stream. During reaction the interfacial In<sup>3+</sup>–O–Ti<sup>4+</sup> sites were first reduced in presence of H<sub>2</sub> and then oxidized back with CO<sub>2</sub> producing CO. Because of the redox mechanism, methanol and methane formation was limited. This study shows the development of a promoter free oxide catalyst for CO<sub>2</sub> hydrogenation and the importance of the redox property at the oxidic interface for selective hydrogenation of CO<sub>2</sub> to CO under unfavorable conditions.

## Introduction

Hydrogenation of CO<sub>2</sub> is an attractive way to produce chemicals and fuels without using fossil resources. Production of CO by partial reduction of CO<sub>2</sub>, also known as reverse water gas shift (RWGS) reaction (Equation 1), is of interest because the conversion of CO to hydrocarbon fuels and useful chemicals through Fischer-Tropsch synthesis (FTS) is already industrially established.<sup>[1–5]</sup> Usual operating condition for RWGS is above 500 °C and atmospheric pressure.<sup>[4]</sup> Under these conditions several catalysts have been reported for RWGS that achieve high CO yield.<sup>[6,7]</sup> However, to effectively couple the two processes, the condition of RWGS reaction should match the subsequent FTS reaction, which is conducted at less than 400 °C and under a pressure of 1–3 MPa.<sup>[8]</sup> At lower temperature and high pressure CO selectivity reduces because RWGS reaction is endothermic in nature and formation of methanol and methane is favored.<sup>[9]</sup> Therefore, it is important to develop efficient catalysts that are selective for CO formation under unfavorable conditions of low temperature and high pressure to match with the subsequent FTS processes.



Noble metal-based catalysts containing Pt has been reported for RWGS at low temperature. For example, Pt/mullite and PtCo/TiO<sub>2</sub> catalysts showed high selectivity of CO with

activity of 12.5 and 11.4 μmol g<sup>-1</sup> s<sup>-1</sup>, respectively.<sup>[10,11]</sup> Single atom Pt catalysts are used to increase the atom efficiency of Pt metal. However, cost of noble metals is prohibitive and they are prone to deactivation due to aggregation of metal sites.<sup>[12–14]</sup> Non-noble metal catalysts containing Ni or Co tend to produce CH<sub>4</sub> and higher hydrocarbons instead of CO.<sup>[15–17]</sup> Cu based catalysts are the exception because of their high activity for RWGS at low temperatures. In particular, Cu supported on reducible supports, especially CeO<sub>2</sub> catalysts, are comparable to noble metals based catalyst for RWGS.<sup>[18–24]</sup> Cu supported over hollow nanosphere of CeO<sub>2</sub> containing high density of oxygen vacancy produced 55 μmol g<sup>-1</sup> s<sup>-1</sup> of CO at 350 °C.<sup>[23]</sup> Similarly, Cu/CeO<sub>2</sub> catalyst derived from pyrolysis of a copper containing metal organic framework (MOF), produced CO at a rate of ca. 9.5 μmol g<sup>-1</sup> s<sup>-1</sup> at 400 °C. Despite the excellent activity achieved by supported Cu catalysts they are prone to deactivation. For example, MOF derived Cu/CeO<sub>2</sub> catalyst lost 25% of activity within the first 24 h.<sup>[18]</sup> The cause of deactivation in Cu catalysts is aggregation of Cu metal particles.<sup>[25,26]</sup> Mixed metal oxide catalysts are considered as promising alternatives because they are stable under CO<sub>2</sub> hydrogenation condition. Oxygen vacancy on the interface of mixed oxide adsorbs and activates CO<sub>2</sub>. However, the interfacial sites promote deep hydrogenation of CO<sub>2</sub> to CH<sub>3</sub>OH and CH<sub>4</sub> because the oxophilic vacancy tends to stabilize the reaction intermediates such as formate and methoxy species.<sup>[27,28]</sup>

In this work, we report the synthesis of an In-TiO<sub>2</sub> mixed oxide catalyst for RWGS reaction by doping In in TiO<sub>2</sub>. In atoms were atomically dispersed throughout the anatase TiO<sub>2</sub> framework. In–O–Ti interfacial site was partially reduced under CO<sub>2</sub> hydrogenation condition and acted as a redox center for CO<sub>2</sub> hydrogenation to CO. The reducibility and oxidizability of both In and Ti at the interfacial site facilitated the redox mechanism leading to high activity and CO selectivity. Indium doped TiO<sub>2</sub> produced CO with >99% selectivity with high yield. CO selectivity did not reduce even under high pressure.

## Results and Discussion

### Catalyst synthesis and characterization

## RESEARCH ARTICLE

Initially, two types of catalyst with interfacial In–O–Ti sites were synthesized by doping indium in titania (In–TiO<sub>2</sub>) and by doping titanium in In<sub>2</sub>O<sub>3</sub> (Ti–In<sub>2</sub>O<sub>3</sub>). Both catalysts were prepared by mixing In and Ti precursors with citric acid to form a sol that was dried and calcined to obtain the doped oxides. The atomic ratio of In:Ti in In–TiO<sub>2</sub> was 1:28 (corresponding to 5 wt.% In loading) and the atomic ratio of Ti:In in Ti–In<sub>2</sub>O<sub>3</sub> was also 1:28. Doping of In and Ti had little influence on the physical structure of their parent bulk oxides. Titania showed anatase crystal phase in In–TiO<sub>2</sub>, which was same as undoped TiO<sub>2</sub> that was also prepared by the sol gel method (Figure 1a). Conversely, In<sub>2</sub>O<sub>3</sub> exhibited cubic phase in Ti–In<sub>2</sub>O<sub>3</sub>, same as undoped In<sub>2</sub>O<sub>3</sub>. No crystal peak of dopant

oxides was observed in both the doped catalysts. Doped oxides showed shifting of XRD peak as compared to their undoped analogues (Figure S1). When In was doped into TiO<sub>2</sub>, the interplanar distance increases because In<sup>3+</sup> (0.8 Å) is larger than Ti<sup>4+</sup> (0.6 Å). As a result, 2θ value of In–TiO<sub>2</sub> XRD patterns decreased as compared to undoped TiO<sub>2</sub> (Figure S1a). Due to the same reason, the XRD patterns of Ti–In<sub>2</sub>O<sub>3</sub> shifted towards higher 2θ value as compared to undoped In<sub>2</sub>O<sub>3</sub> (Figure S1b). The doped catalysts also showed similar N<sub>2</sub> adsorption isotherms and surface area as compared to their undoped counterpart oxides (Figure 1b and Table S1).

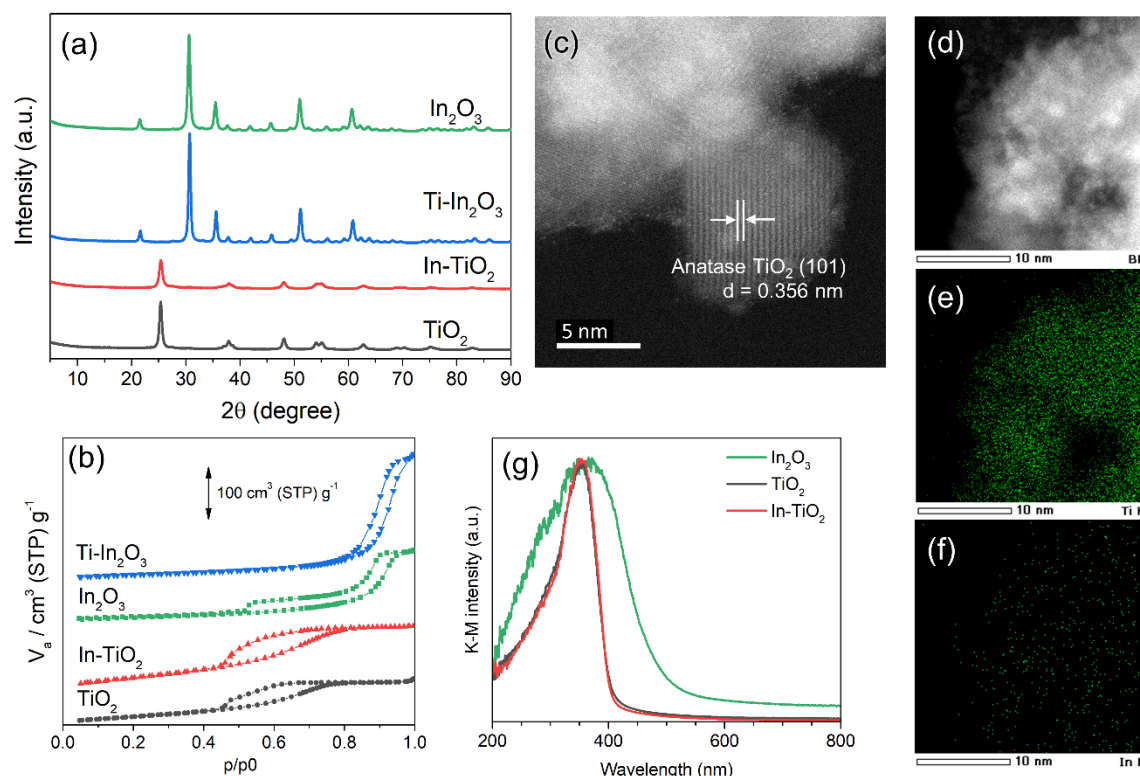


**Figure 1.** (a) XRD pattern of In–TiO<sub>2</sub> and Ti–In<sub>2</sub>O<sub>3</sub> doped catalyst along with undoped single oxides. (b) N<sub>2</sub> adsorption isotherms of In–TiO<sub>2</sub>, Ti–In<sub>2</sub>O<sub>3</sub> and undoped analogues. (c) HAADF-STEM image of In–TiO<sub>2</sub> showing anatase crystal structure of TiO<sub>2</sub>. EDX elemental mapping of the selected region (d) showing the homogeneous distribution of (e) Ti and (f) In. (g) Diffuse reflectance UV-Vis absorption spectra of In–TiO<sub>2</sub> compared with undoped TiO<sub>2</sub> and In<sub>2</sub>O<sub>3</sub>.

Further characterization showed that the dopants were highly dispersed without agglomeration. In the high-angle annular dark field scanning transmission electron microscopy (HAADF-STEM) analysis of In–TiO<sub>2</sub> (Figure 1c), only anatase titania phase was observed. In was highly dispersed in TiO<sub>2</sub> as seen in elemental mapping by energy dispersive X-ray (EDX) analysis (Figure 1d-f). Also, the results from diffuse reflectance UV-Vis absorption spectroscopy show that In was atomically dispersed in In–TiO<sub>2</sub>. In the UV-Vis spectra absorption peak at 340 nm was observed corresponding to the electronic transition from valence band to conduction band for anatase titania (Figure 1g).<sup>[29]</sup> Features indicating formation of In<sub>2</sub>O<sub>3</sub> crystals, such as electronic transition from valence band to conduction band and broadening until 600 nm, were not present.<sup>[30]</sup>

Similar to In–TiO<sub>2</sub>, HAADF-STEM image of Ti–In<sub>2</sub>O<sub>3</sub> (Figure S2a) showed cubic In<sub>2</sub>O<sub>3</sub> and TiO<sub>2</sub> was not observed. Highly dispersed Ti was observed in the elemental mapping analysis (Figure S2b-d). In the UV-Vis analysis, the absorption peak position for Ti–In<sub>2</sub>O<sub>3</sub> was shifted towards lower wavenumber as compared to undoped In<sub>2</sub>O<sub>3</sub> due to the doping of Ti in In<sub>2</sub>O<sub>3</sub>

(Figure S3).<sup>[31]</sup> These results show that mixed oxide of In–TiO<sub>2</sub> and Ti–In<sub>2</sub>O<sub>3</sub> were formed and the dopant was dispersed in the parent oxide without formation of agglomerated particles.

### Catalytic activity

After confirming the formation of mixed oxide containing interfacial In–O–Ti sites, these catalysts were tested for CO<sub>2</sub> hydrogenation reaction in a fixed bed flow reactor at 300 °C, 3 MPa, 30,000 mL h<sup>-1</sup> g<sub>cat</sub><sup>-1</sup>, H<sub>2</sub>:CO<sub>2</sub> = 3:1. In the presence of In–TiO<sub>2</sub> catalyst, CO<sub>2</sub> conversion was 7.4% with CO selectivity of more than 99% with traces of CH<sub>4</sub> (Figure 2a). Undoped TiO<sub>2</sub> showed negligible CO<sub>2</sub> conversion of 0.1%. Therefore, doping indium in TiO<sub>2</sub> enhanced its activity for CO<sub>2</sub> hydrogenation while favoring CO as the only product. For Ti–In<sub>2</sub>O<sub>3</sub> catalyst, CO selectivity was 70% along with 4.6% CO<sub>2</sub> conversion. In contrast, undoped In<sub>2</sub>O<sub>3</sub> produced methanol as the primary product with a selectivity of 54% and CO<sub>2</sub> conversion of 4.4%. Because Ti–In<sub>2</sub>O<sub>3</sub> and undoped In<sub>2</sub>O<sub>3</sub> had similar surface area and they showed similar CO<sub>2</sub> conversion, the shift in selectivity from methanol to

## RESEARCH ARTICLE

CO was attributed to doping of Ti in  $\text{In}_2\text{O}_3$ . Therefore, presence of In–O–Ti interfacial site favored the formation of CO in Ti– $\text{In}_2\text{O}_3$  and In– $\text{TiO}_2$  catalysts.

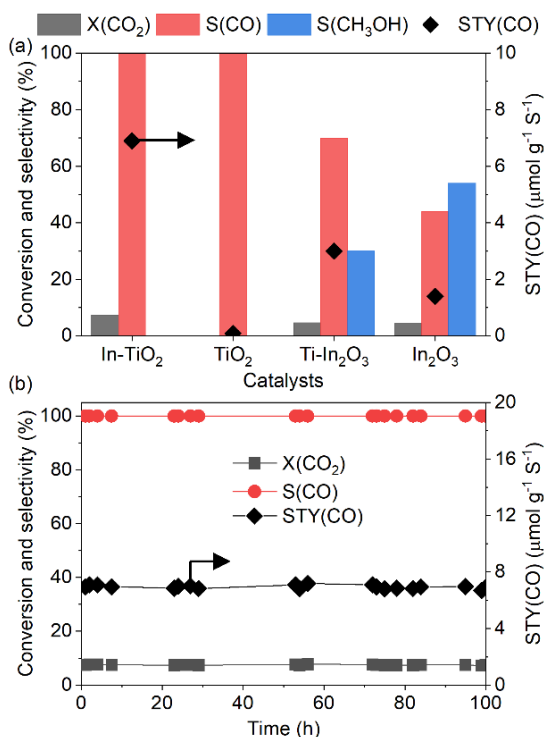


**Figure 2.** (a) Comparison of  $\text{CO}_2$  hydrogenation activity of different catalysts. (b) Long term stability of In– $\text{TiO}_2$  during  $\text{CO}_2$  hydrogenation. Reaction condition: 300 °C, 3 MPa, 30000 mL h<sup>-1</sup> g<sup>-1</sup>,  $\text{H}_2$ : $\text{CO}_2$  = 3:1.

Further optimization of reaction condition over In– $\text{TiO}_2$  showed that the selective formation of CO was independent of hydrogenation reaction condition. Increasing the temperature to 350 °C increased the  $\text{CO}_2$  conversion from 7.4% to 19.5% without any change in CO selectivity (Table 1). Typically, CO selectivity in RWGS reaction is favored at high temperature and low pressure.<sup>[32–34]</sup> In contrast, CO selectivity was more than 99% over In– $\text{TiO}_2$  irrespective of change in pressure, temperature and space velocity. At 350 °C and 3 MPa, the CO space time yield (STY) was 18 μmol g<sup>-1</sup> s<sup>-1</sup>, which was comparable to that of noble

metal-based catalysts under similar reaction condition (Table S2). At an SV of 60,000 the STY increased to 22 μmol g<sup>-1</sup> s<sup>-1</sup>. The catalyst was stable in long term reaction and did not show any loss in activity or selectivity after 100 h on stream (Figure 2b). Therefore, interfacial In–O–Ti sites formed on In– $\text{TiO}_2$  showed remarkable activity and stability for selectively converting  $\text{CO}_2$  to CO over a wide range of reaction condition.

**Table 1.** Activity of In– $\text{TiO}_2$  catalyst at different reaction conditions.<sup>[a]</sup>

T (°C)	P (MPa)	SV (ml h <sup>-1</sup> g <sup>-1</sup> )	$\text{CO}_2$ Conv. (%)	CO Sel. (%)	STY (μmol g <sup>-1</sup> s <sup>-1</sup> )
300	0.1	30,000	1.0	100	0.98
300	3	30,000	7.4	>99	6.9
350	3	30,000	19.5	>99	18
350	3	60,000 <sup>[b]</sup>	11.7	>99	22

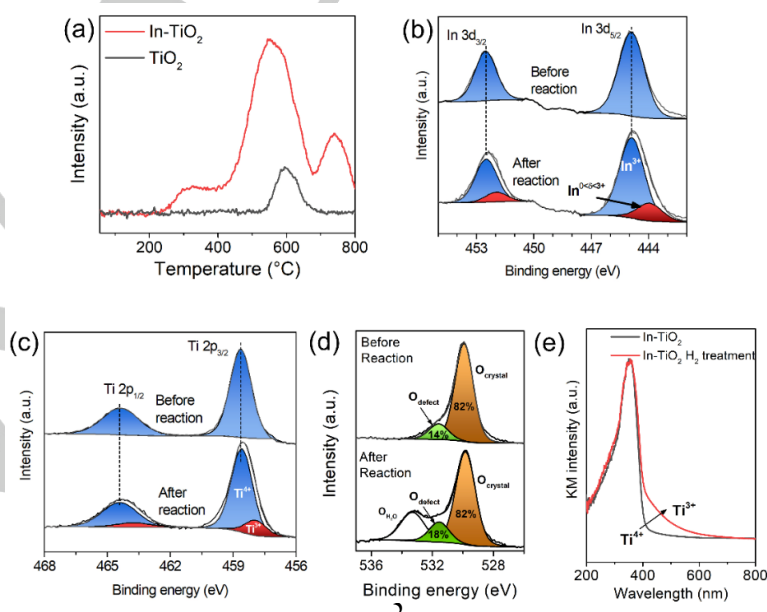
<sup>[a]</sup>Catalyst: In– $\text{TiO}_2$  200 mg,  $\text{H}_2$ : $\text{CO}_2$  = 3:1.

<sup>[b]</sup>Catalyst amount was halved to 100 mg.

### Mechanistic Clarification

After confirming the presence of interfacial In–O–Ti active site and its high activity for CO production, In– $\text{TiO}_2$  catalyst was further analyzed to ascertain the mechanism of CO formation and the role of surface interface. Doping of In increased the  $\text{H}_2$  dissociation ability of catalysts at lower temperature (Figure 3a). Undoped  $\text{TiO}_2$  showed little  $\text{H}_2$  consumption below 550 °C during temperature programmed reduction (TPR) under  $\text{H}_2$  flow.  $\text{H}_2$  consumption in the temperature range of 250–400 °C was observed for In– $\text{TiO}_2$  catalyst, which was assigned to reduction of In–O–Ti interface.

Above 500 °C, surface indium atoms underwent complete reduction to form metal nanoparticles. This was evidenced by XRD of In– $\text{TiO}_2$  treated at 550 °C under  $\text{H}_2$  (Figure S4). Above 700 °C anatase  $\text{TiO}_2$  transformed to rutile phase. In the XRD spectrum of sample treated at 700 °C metallic In nanoparticle peak increased in size as In withing the bulk crystal also reduced during phase transition of  $\text{TiO}_2$  (Figure S4).



## RESEARCH ARTICLE

**Figure 3.** (a) H<sub>2</sub> TPR spectra of In–TiO<sub>2</sub> and undoped TiO<sub>2</sub>. (b), (c), and (d) XPS spectra of In–TiO<sub>2</sub> catalyst before and after CO<sub>2</sub> hydrogenation for In 3d, Ti 2p and O 1s regions, respectively. (e) UV-Vis analysis for In–TiO<sub>2</sub> before and after treatment under H<sub>2</sub> atmosphere at 350 °C showing formation of Ti<sup>3+</sup> species.

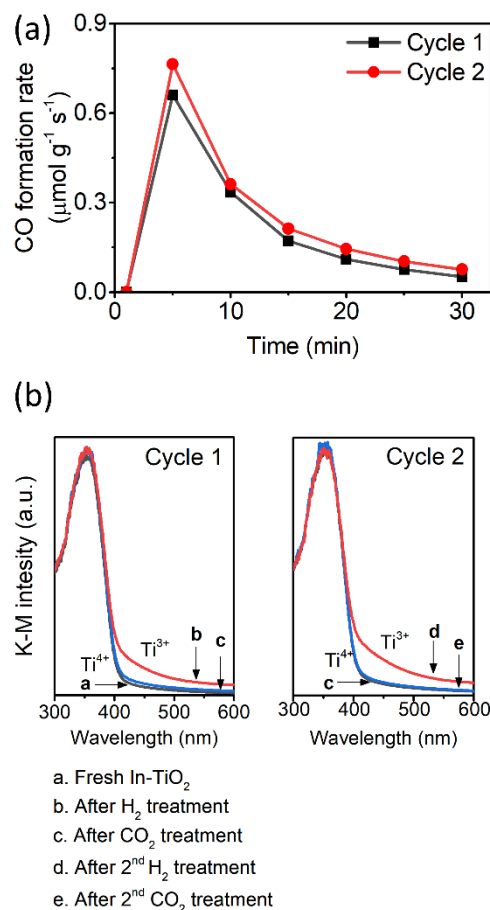
The partial reduction of In–O–Ti interfacial sites at low temperature (below 400 °C) was evident from ex-situ X-ray photoelectron spectroscopy (XPS) and UV-Vis analysis. In XPS analysis of In–TiO<sub>2</sub> catalyst after CO<sub>2</sub> hydrogenation reaction, a peak for partially reduced In species was present at 443.9 eV (Figure 3b).<sup>[35]</sup> Similarly, in the Ti 2p XPS spectra, presence of Ti<sup>3+</sup> at 458 eV in the used catalyst was also observed (Figure 3c).<sup>[36,37]</sup> This suggests that during reaction, both In<sup>3+</sup> and Ti<sup>4+</sup> present at the interface were partially reduced. As a result, an increase in oxygen defects was observed in the O 1s XPS spectra from 14% to 18% (Figure 3d). In the UV-Vis spectrum for In–TiO<sub>2</sub> a broad shoulder appeared in the range of 400–700 nm after treating the catalyst under H<sub>2</sub> at 350 °C (Figure 3e). This shoulder was assigned to formation of Ti<sup>3+</sup> species due to reduction of the metal oxide interface.<sup>[29,38]</sup> Similar shoulder did not appear when undoped TiO<sub>2</sub> was subjected to H<sub>2</sub> treatment (Figure S5). Therefore, In–O–Ti interface underwent reduction during the reaction to form In<sup>0<δ<3+</sup>–V<sub>o</sub>–Ti<sup>3+</sup>, where V<sub>o</sub> denotes an oxygen vacancy.

Oxide catalysts bearing oxygen vacancies are known to strongly adsorb CO<sub>2</sub>, which increases their catalytic activity.<sup>[39]</sup> Such CO<sub>2</sub> species, present in bent or carbonate form, undergo hydrogenation to form formate or carboxyl intermediate via associated mechanism. In a CO<sub>2</sub> temperature programmed desorption (TPD) these species desorb at temperatures above 300 °C.<sup>[39]</sup> However, TPD of CO<sub>2</sub> adsorbed over H<sub>2</sub> pretreated In–TiO<sub>2</sub> only exhibited CO<sub>2</sub> desorption peak at 120 °C assigned to physisorbed and weakly adsorbed CO<sub>2</sub> species (Figure S6a). There was negligible desorption of CO<sub>2</sub> above 300 °C indicating absence of strongly adsorbed CO<sub>2</sub> species necessary for CO<sub>2</sub> conversion by associated mechanism. Investigation of adsorbed CO<sub>2</sub> species using diffuse reflectance infrared Fourier transform spectroscopy (DRIFTS) further confirmed that bicarbonate and carbonate species formed during room temperature adsorption of CO<sub>2</sub> disappeared before 250 °C and such species were not detected at 350 °C (Figure S6b). When the DRIFTS experiment was performed under in-situ conditions, intermediate species of RWGS reaction such as formate or carboxyl were not detected over In–TiO<sub>2</sub> catalyst and only peaks for gaseous CO were observed at 2172 and 2109 cm<sup>-1</sup> (Figure S7).<sup>[40]</sup> Over In<sub>2</sub>O<sub>3</sub>, carboxyl and formate species are known to be the intermediates for methanol and CO formation through the association mechanism.<sup>[41]</sup> Therefore, the formation of CO without the presence of any intermediate indicated that CO might be produced via, redox mechanism (also called reverse Mars-van Krevelen mechanism), where H<sub>2</sub> reduces the In–O–Ti interface and CO<sub>2</sub> directly oxidizes the interface to produce CO.

To confirm the redox nature of mechanism, In–TiO<sub>2</sub> was first treated with H<sub>2</sub> at 300 °C for 15 min and then purged with Ar to remove the residual H<sub>2</sub> gas. Then a mixture of Ar and CO<sub>2</sub> was passed over the catalyst and the evolution of CO was recorded using a GC. CO evolution was observed for more than 20 min even in the absence of H<sub>2</sub> (Figure 4a). Repeating the reduction and oxidation cycle a second time gave identical result. In contrast, when undoped In<sub>2</sub>O<sub>3</sub> catalyst was used, product evolution was poor (Figure S8). The redox cycle of In–TiO<sub>2</sub> catalyst was also observed ex-situ by UV-VIS spectroscopy after each reduction and oxidation cycle (Figure 4b). Formation of Ti<sup>3+</sup> species was apparent after the first reduction step owing to the appearance of

broad shoulder at 400–500 nm<sup>-1</sup> (Figure 4b, spectra a and b)). After CO<sub>2</sub> treatment the intensity of the Ti<sup>3+</sup> shoulder reduced in UV-Vis spectrum (Figure 4b, spectrum c). This phenomenon was reversible under repetitive reduction and oxidation cycles (Figure 4b, spectra c–e). Therefore, we conclude that In–TiO<sub>2</sub> catalyzed CO<sub>2</sub> reduction to CO through reverse Mars-van Krevelen mechanism, at the interface of In and Ti atoms.

**Figure 4.** (a) Rate of CO production over pre-reduced In–TiO<sub>2</sub> when flowing

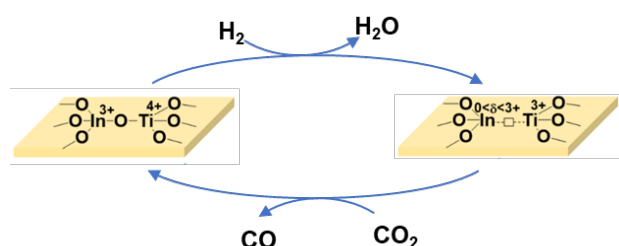


CO<sub>2</sub> in the absence of H<sub>2</sub> at 300 °C. For each cycle catalyst was first reduced with H<sub>2</sub> at 300 °C before flowing CO<sub>2</sub>. (b) UV-Vis spectra of In–TiO<sub>2</sub> catalyst after successive treatment with H<sub>2</sub> and CO<sub>2</sub> showing transition between Ti<sup>4+</sup> and Ti<sup>3+</sup> species over the surface.

Scheme 1 depicts the mechanism for CO<sub>2</sub> hydrogenation over the surface of In–TiO<sub>2</sub>. Catalyst characterization has shown that doping In in TiO<sub>2</sub> enhances reduction of the catalyst surface under the reaction condition. Formation of partially reduced In species and Ti<sup>3+</sup> confirms the reduction of In<sup>3+</sup>–O–Ti<sup>4+</sup> interfacial site. Although the surface reduction generated oxygen vacancy, it did not cause chemisorption of CO<sub>2</sub> on the catalyst surface favorable for formate or carboxyl formation. Instead, the partially reduced In and Ti<sup>3+</sup> at the interfacial site interacted with the O of CO<sub>2</sub> and they were oxidized by CO<sub>2</sub>. The oxygen deficient site is replenished to recover In<sup>3+</sup>–O–Ti<sup>4+</sup> species and CO was produced and removed from the catalyst surface. Because intermediates were not formed during the reaction their subsequent hydrogenation to methane or methanol was less likely. Furthermore, owing to high dispersion of In species and lack of

## RESEARCH ARTICLE

metal nanoparticles, hydrogenation of CO to methane was suppressed. Consequently, high CO selectivity was maintained even at low temperature and high pressure, which are favorable for methane formation. The reversibility of the In–O–Ti interface for redox reaction without undergoing over reduction ensured the stability of the catalyst.



**Scheme 1.** Catalytic CO<sub>2</sub> hydrogenation to CO over In–TiO<sub>2</sub> catalyst through reverse Mars-van Krevelen pathway.

## Conclusion

In summary, we show that doping of In into TiO<sub>2</sub> led to the formation of highly active and selective interfacial active site for the RWGS reaction. The activity of CO production over In–TiO<sub>2</sub> catalyst was comparable to noble metal-based catalysts. More than 99% selectivity of CO was obtained 350 °C and 3MPa pressure. Under the reaction condition, interfacial In<sup>3+</sup>–O–Ti<sup>4+</sup> site was first reduced in presence of H<sub>2</sub> to form In<sup>0<δ<3+</sup>–V<sub>o</sub>–Ti<sup>3+</sup> and then oxidized back with CO<sub>2</sub> producing CO. Consequently, the reaction proceeded through reverse Mars-van Krevelen mechanism. The formation of methane was suppressed because of lack of metal nanoparticles to catalyze hydrogenation of CO. As a result, RWGS reaction was possible at conditions similar to Fischer-Tropsch synthesis. The redox property at the interfacial site shown in this study can also be applied to reactions other than CO<sub>2</sub> hydrogenation and can help in the development of promoter free oxide catalysts for redox reactions.

## Experimental Section

### Catalyst preparation

Indium nitrate (In(NO<sub>3</sub>)<sub>3</sub>·3H<sub>2</sub>O), aqueous titanium chloride solution (aqueous solution of 20% TiCl<sub>3</sub> containing 5% HCl) and citric acid were purchased from Fujifilm Wako Pure Chemical Corporation. All catalysts were prepared using a sol-gel method in the presence of citric acid. A typical procedure to obtain In–TiO<sub>2</sub> catalysts is as follows: In(NO<sub>3</sub>)<sub>3</sub>·3H<sub>2</sub>O (0.435 mmol) and TiCl<sub>3</sub> (12.5 mmol) solution were added to a beaker containing 60 mL of H<sub>2</sub>O along with 20 mmol of citric acid. The beaker was placed on a hot plate maintained at 150 °C and stirred until a foaming gel was formed. The gel was then dried in an oven maintained at 150 °C for 5 h. The resulting composite was crushed and calcined at 500 °C for 3 h (ramp rate: 2 °C min<sup>-1</sup>) to obtain the final catalyst. For Ti–In<sub>2</sub>O<sub>3</sub>, 0.453 mmol of TiCl<sub>3</sub> and 12.5 mmol of In(NO<sub>3</sub>)<sub>3</sub>·3H<sub>2</sub>O were used and same method was followed. Undoped oxides were prepared in the same manner without the presence of the dopant.

### Catalyst Characterization

X-ray diffraction (XRD) pattern was measured with Rigaku MiniFlex using CuKα X-ray (λ = 1.54 Å) operating at 40 kV and 20 mA. N<sub>2</sub> adsorption

isotherms were measured at –196 °C using a Belsorp mini analyzer. Prior to the adsorption, all samples were degassed under vacuum at 120 °C for 2 h. Surface area was calculated by using BET theory between the relative pressure range 0.05 to 0.35 in the N<sub>2</sub> adsorption isotherm. X-ray photoelectron spectroscopy (XPS) was performed with JEOL JPS-9010MC instrument. Charge correction was done by adjusting the carbon peak to 284.6 eV. STEM images were obtained in a JEOL JEM-ARM200F atomic resolution electron microscope at an acceleration voltage of 200 kV equipped with EDS detector EX-24221M1G5T. Temperature programmed reduction (TPR) of catalysts was carried out in presence of H<sub>2</sub>-Ar mixture (H<sub>2</sub> = 5%) in a BELCAT II instrument equipped with a TCD detector. Prior to measurement, catalysts were pretreated at 200 °C for 1 hour under Ar flow. Measurements were done at a total flow rate of 50 mL min<sup>-1</sup> with ramp rate of 10 °C min<sup>-1</sup>. CO<sub>2</sub> TPD experiment was performed in the BELCAT II instrument equipped with BELMass gas mass spectrometer. Prior to measurement, the samples were pretreated under He at 200 °C for 60 min followed by CO<sub>2</sub> adsorption at room temperature for 30 min. After purging with He for 30 min TPD was performed with a ramp rate of 10 °C min<sup>-1</sup>. DRIFTS experiments were done using a Perkin Elmer Spectrum 100 FTIR spectrometer equipped with MCT detector cooled with liquid N<sub>2</sub>. The catalyst was first pretreated under He at 300 °C for 30 min. One spectrum of catalyst was recorded as background under He before flowing reactant gases (H<sub>2</sub>:CO<sub>2</sub> = 3). Final IR spectrum of the adsorbed species was obtained by subtracting the background spectrum of the catalyst. The UV-Vis analysis was carried out in a JASCO V-650 spectrophotometer. To check the redox property of the catalyst in the reactor, first the catalyst was reduced under H<sub>2</sub> for 15 min at 300 °C followed by the Ar flow to remove H<sub>2</sub> gas. Then the catalyst was treated with a mixture of Ar and CO<sub>2</sub> and the evolution of CO was recorded in GC-TCD. This whole procedure was repeated on the same catalyst bed to ensure the reproducibility of the redox process. The UV-Vis analysis of the redox process was done by treating the same batch of catalyst under different atmospheres and quickly analyzing the treated catalyst in the spectrophotometer. For comparison between different samples, peak intensities were normalized according to the primary peak intensity of undoped TiO<sub>2</sub>.

### Evaluation of catalytic activity

Catalytic activity for CO<sub>2</sub> hydrogenation was evaluated in a stainless-steel fixed bed flow reactor system. Products were analyzed using an online GC (Shimadzu, GC 8A) equipped with two columns – Porapak Q and Molecular Sieve and a TCD detector. Gas line from the outlet of the reactor to the inlet of the GC was heated at 150 °C to prevent condensation. Typically, 200 mg of catalyst was loaded into the reactor and held in place by quartz wool. A thermocouple was inserted into the reactor to measure catalyst bed temperature. The reactor was pressurized to reaction condition using a mixture of H<sub>2</sub> and CO<sub>2</sub> having the ratio H<sub>2</sub>:CO<sub>2</sub> = 3:1. After the system pressure was stable, reactor temperature was increased to desired value. Total flow rate was 100 mL min<sup>-1</sup> to maintain space velocity at 30,000 mL h<sup>-1</sup> g<sup>-1</sup>. Reactions at space velocity higher than 30,000 mL h<sup>-1</sup> g<sup>-1</sup> were carried out by reducing the amount of catalyst.

CO<sub>2</sub> conversion, selectivity of CO and CH<sub>3</sub>OH and space time yield (STY) of CH<sub>3</sub>OH were calculated using the following equations.

CO<sub>2</sub> conversion (equation 2):

$$X_{(CO_2)} = \left( \frac{nCO_{out} + nCH_3OH_{out} + nCH_4_{out}}{nCO_{in} + nCO_{out} + nCH_3OH_{out} + nCH_4_{out}} \right) \times 100\% \quad (2)$$

CO and CH<sub>3</sub>OH selectivity (equation 3-4)

$$S_{(CO)} = \left( \frac{nCO_{out}}{nCO_{out} + nCH_3OH_{out} + nCH_4_{out}} \right) \times 100\% \quad (3)$$

$$S_{(CH_3OH)} = \left( \frac{nCH_3OH_{out}}{nCO_{out} + nCH_3OH_{out} + nCH_4_{out}} \right) \times 100\% \quad (4)$$

## RESEARCH ARTICLE

Space time yield (STY) of CO (equation 5):

$$STY_{(CO)} = \left( \frac{SV \times [CO_2] \times X_{(CO_2)} \times S_{(CO)}}{224 \times 3600} \right) \quad (5)$$

Where  $n_{CO_{2out}}$ ,  $n_{CO_{out}}$ ,  $n_{CH_3OH_{out}}$ ,  $n_{CH_4_{out}}$  are moles of  $CO_2$ ,  $CO$ ,  $CH_3OH$  and  $CH_4$  calculated from GC analysis.  $SV$  is space velocity in  $mL\ h^{-1}\ g^{-1}$ ,  $[CO_2]$  is the concentration of  $CO_2$  present in the feed gas mixture in %. STY of CO is reported in  $\mu mol\ g^{-1}\ s^{-1}$ .

## Acknowledgements

This work was supported by JSPS Grant-in-Aid for Scientific Research (C) KAKENHI JP22K04821.

## Conflict of Interest

The authors declare no conflict of interest.

## Data availability Statement

The data that support the findings of this study are available from the corresponding author upon reasonable request.

**Keywords:**  $CO_2$  hydrogenation, reverse water gas shift, redox, mixed oxide, reverse Mars-van Krevelen mechanism

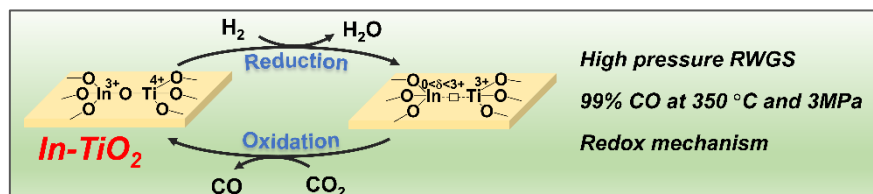
- [1] J. Qi, J. Finzel, H. Robotjazi, M. Xu, A. S. Hoffman, S. R. Bare, X. Pan, P. Christopher, *J. Am. Chem. Soc.* **2020**, *142*, 14178–14189.
- [2] Y. Li, W. Gao, M. Peng, J. Zhang, J. Sun, Y. Xu, S. Hong, X. Liu, X. Liu, M. Wei, B. Zhang, D. Ma, *Nat. Commun.* **2020**, *11*, 1–8.
- [3] S. Lyu, L. Wang, Z. Li, S. Yin, J. Chen, Y. Zhang, J. Li, Y. Wang, *Nat. Commun.* **2020**, *11*, 1–8.
- [4] J. Bao, G. Yang, Y. Yoneyama, N. Tsubaki, *ACS Catal.* **2019**, *9*, 3026–3053.
- [5] J. Li, Y. He, L. Tan, P. Zhang, X. Peng, A. Oruganti, G. Yang, H. Abe, Y. Wang, N. Tsubaki, *Nat. Catal.* **2018**, *1*, 787–793.
- [6] H.-X. Liu, S.-Q. Li, W.-W. Wang, W.-Z. Yu, W.-J. Zhang, C. Ma, C.-J. Jia, *Nat. Commun.* **2022**, *13*, 867.
- [7] P. C. Zonetti, S. Letichevsky, A. B. Gaspar, E. F. Sousa-Aguiar, L. G. Appel, *Appl. Catal. A Gen.* **2014**, *475*, 48–54.
- [8] Q. Zhang, J. Kang, Y. Wang, *ChemCatChem* **2010**, *2*, 1030–1058.
- [9] X. Jiang, X. Nie, X. Guo, C. Song, J. G. Chen, *Chem. Rev.* **2020**, *120*, 7984–8034.
- [10] B. Liang, H. Duan, X. Su, X. Chen, Y. Huang, X. Chen, J. J. Delgado, T. Zhang, *Catal. Today* **2017**, *281*, 319–326.
- [11] S. Kattel, W. Yu, X. Yang, B. Yan, Y. Huang, W. Wan, P. Liu, J. G. Chen, *Angew. Chemie - Int. Ed.* **2016**, *55*, 7968–7973.
- [12] A. Goguet, F. Meunier, J. P. Breen, R. Burch, M. I. Petch, A. Faur Ghenciu, *J. Catal.* **2004**, *226*, 382–392.
- [13] S. Mine, T. Yamaguchi, K. W. Ting, Z. Maeno, S. M. A. H. Siddiki, K. Oshima, S. Satokawa, K. I. Shimizu, T. Toyao, *Catal. Sci. Technol.* **2021**, *11*, 4172–4180.
- [14] L. Chen, R. R. Unocic, A. S. Hoffman, J. Hong, A. H. Braga, Z. Bao, S. R. Bare, J. Szanyi, *JACS Au* **2021**, *1*, 977–986.
- [15] J. Zhu, G. Zhang, W. Li, X. Zhang, F. Ding, C. Song, X. Guo, *ACS Catal.* **2020**, *15*, 57.
- [16] A. Parastaev, V. Muravev, E. Huertas Osta, A. J. F. van Hoof, T. F. Kimpel, N. Kosinov, E. J. M. Hensen, *Nat. Catal.* **2020**, *3*, 526–533.
- [17] J. Li, Y. Lin, X. Pan, D. Miao, D. Ding, Y. Cui, J. Dong, X. Bao, *ACS Catal.* **2019**, *9*, 6342–6348.
- [18] M. Ronda-Lloret, S. Rico-Francés, A. Sepúlveda-Escribano, E. V. Ramos-Fernandez, *Appl. Catal. A Gen.* **2018**, *562*, 28–36.
- [19] L. Chen, D. Wu, C. Wang, M. Ji, Z. Wu, *J. Environ. Chem. Eng.* **2021**, *9*, 105183.
- [20] G. Zhou, F. Xie, L. Deng, G. Zhang, H. Xie, *Int. J. Hydrogen Energy* **2020**, *45*, 11380–11393.
- [21] L. Lin, S. Yao, Z. Liu, F. Zhang, N. Li, D. Vovchok, A. Martínez-Arias, R. Castaneda, J. Lin, S. D. Senanayake, D. Su, D. Ma, J. A. Rodriguez, *J. Phys. Chem. C* **2018**, *122*, 12934–12943.
- [22] S. C. Yang, S. H. Pang, T. P. Sulmonetti, W. N. Su, J. F. Lee, B. J. Hwang, C. W. Jones, *ACS Catal.* **2018**, *8*, 12056–12066.
- [23] Y. Zhang, L. Liang, Z. Chen, J. Wen, W. Zhong, S. Zou, M. Fu, L. Chen, D. Ye, *Appl. Surf. Sci.* **2020**, *516*, 146035.
- [24] C. S. Chen, J. H. Lin, J. H. You, C. R. Chen, *J. Am. Chem. Soc.* **2006**, *128*, 15950–15951.
- [25] D. Vovchok, C. Zhang, S. Hwang, L. Jiao, F. Zhang, Z. Liu, S. D. Senanayake, J. A. Rodriguez, *ACS Catal.* **2020**, *10*, 10216–10228.
- [26] M. V. Twigg, M. S. Spencer, *Appl. Catal. A Gen.* **2001**, *212*, 161–174.
- [27] J. Wang, C. Tang, G. Li, Z. Han, Z. Li, H. Liu, F. Cheng, C. Li, *ACS Catal.* **2019**, *9*, 10253–10259.
- [28] J. Wang, G. Li, Z. Li, C. Tang, Z. Feng, H. An, H. Liu, T. Liu, C. Li, *Sci. Adv.* **2017**, *3*, 1–11.
- [29] L. F. Bobadilla, J. L. Santos, S. Ivanova, J. A. Odriozola, A. Urakawa, *ACS Catal.* **2018**, *8*, 7455–7467.
- [30] M. Ziemba, L. Schumacher, C. Hess, *J. Phys. Chem. Lett.* **2021**, *12*, 3749–3754.
- [31] J. Sánchez-Marcos, I. M. Ochando, R. E. Galindo, R. Martínez-Morillas, C. Prieto, *Phys. Status Solidi Appl. Mater. Sci.* **2010**, *207*, 1549–1553.
- [32] S. Roy, A. Cherevotan, S. C. Peter, *ACS Energy Lett.* **2018**, *3*, 1938–1966.
- [33] S. De, A. Dokania, A. Ramirez, J. Gascon, *ACS Catal.* **2020**, *10*, 14147–14185.
- [34] S. Kattel, P. Liu, J. G. Chen, *J. Am. Chem. Soc.* **2017**, *139*, 9739–9754.
- [35] M. M. J. Li, H. Zou, J. Zheng, T. S. Wu, T. S. Chan, Y. L. Soo, X. P. Wu, X. Q. Gong, T. Chen, K. Roy, G. Held, S. C. E. Tsang, *Angew. Chemie - Int. Ed.* **2020**, *59*, 16039–16046.
- [36] G. Liu, H. G. Yang, X. Wang, L. Cheng, H. Lu, L. Wang, G. Q. Lu, H. M. Cheng, *J. Phys. Chem. C* **2009**, *113*, 21784–21788.
- [37] X. Chen, L. Liu, P. Y. Yu, S. S. Mao, *Science* **2011**, *331*, 746–750.
- [38] H. Liu, H. T. Ma, X. Z. Li, W. Z. Li, M. Wu, X. H. Bao, *Chemosphere* **2003**, *50*, 39–46.
- [39] O. Martín, A. J. Martín, C. Mondelli, S. Mitchell, T. F. Segawa, R. Hauert, C. Drouilly, D. Curulla-Ferré, J. Pérez-Ramírez, *Angew. Chemie - Int. Ed.* **2016**, *55*, 6261–6265.

- [40] N. H. M. Dostagir, R. Rattanawan, M. Gao, J. Ota, J. Y. Hasegawa, K. Asakura, A. Fukouka, A. Shrotri, *ACS Catal.* **2021**, *11*, 9450–9461.
- [41] J. Wang, G. Zhang, J. Zhu, X. Zhang, F. Ding, A. Zhang, X. Guo, C. Song, *ACS Catal.* **2021**, *11*, 1406–1423.

WILEY-VCH

## Entry for the Table of Contents

Insert graphic for Table of Contents here.



Reverse water gas shift reaction under unfavorable condition of high pressure and low temperature is reported. 99% CO selectivity with high yield was obtained owing to the redox nature of reaction over easily reducible interface of In-TiO<sub>2</sub> mixed oxide.

Institute and/or researcher Twitter usernames: